Hudson River Park Trust's CUNY Research Alliance Scholars

Report: Microbial ecology and oyster recruitment: chemical and taxonomic properties of microbial mats and effects on reef ball success

Ana Gonzalez-Nayeck,PhD,

June Rahman, Parneet Kaur, Amanda Flores, and Chester Zarnoch, PhD

Baruch College, City University of New York

February 2026

Abstract:

Restoring oyster habitats in the Hudson River is a promising strategy to access the ecosystem services (filtration and habitat provision) that oyster reefs provide. As part of these efforts, the Hudson River Park Trust's (HRPT) River Project deployed two miniature reef balls seeded with oyster spat (juvenile oysters) adjacent to the reconstructed Gansevoort salt marsh in 2024. One reef ball was subtidal and experienced near total oyster mortality, while the other was intertidal and displayed oyster growth. We hypothesized that the high irradiance experienced by intertidal reef balls promotes growth of biofilm with relatively higher proportions of photosynthetic organisms, resulting in higher carbohydrate content and promoting oyster growth. Conversely, we hypothesize that the lower irradiance experienced by submerged reef balls either limits biofilm or promotes growth of biofilm with a lower carbohydrate content, limiting oyster growth. We tested these hypotheses by deploying cured oyster shells attached to intertidal and subtidal miniature reef balls and analyzing the biofilm communities that grow on both the reef balls and shells. Shell and reef ball samples were analyzed for taxonomic composition, and shell biofilms were additionally analyzed for their nitrogen (N) cycling capacity (to determine the efficacy of N removal) and composition of exopolymeric substances (EPS). Photosynthetic microbes were relatively more abundant on intertidal reef balls. However, there was no difference in total oyster growth or N cycling rates between intertidal and subtidal reef balls in 2025, and preliminary results suggest intertidal biofilms contain less bulk EPS than subtidal biofilm. Thus, we tentatively reject our initial hypothesis. We do note that oyster growth on subtidal reef balls was limited to the upper half of the structure, and that subtidal reef balls contained significantly more strict anaerobic bacteria. As such, we suggest future work investigate the conditions under which hypoxic microzones are created within oyster habitats to better inform optimal reef ball placement for successful oyster growth.

Introduction

The Lower Hudson River Estuary (HRE) is impacted by nutrient pollution, primarily nitrogen (N), leading to excess growth of phytoplankton that can release toxins and promote localized hypoxic conditions (Dianne I. Greenfield, 2023; Howarth et al., 2006). *Crassostrea virginica* (Atlantic

oyster) is native to the HRE and can remediate excess N pollution; however, native oyster populations have remained only minorly abundant since their collapse due to overharvesting in the early 19th century (Coen et al., 2007; Jacques, 2017). Since 2021, the Hudson River Park (henceforth the Park), in partnership with the Billion Oyster Project and U.S. Army Corps of Engineers, has been working towards deploying 300+ large-scale oyster habitats to restore the ecosystem services they provide, including habitat provision and development of flood-resistant living coastlines in addition to their roles in N remediation (Hudson River Park Trust, River Project, 2024).

As part of these efforts, the Hudson River Park Trust's (henceforth the Trust) River Project deployed two miniature reef balls seeded with oyster spat (juvenile oysters) adjacent to the reconstructed Gansevoort salt marsh in 2024 as small-scale replicas that can be more closely monitored relative to the larger, less accessible structures. In 2024, one reef ball was submerged and experienced near total oyster mortality, while the other was intermittently exposed (intertidal) and displayed oyster growth (Hudson River Park Trust, River Project, 2024). The surface of an intertidal reef ball experiences high irradiance and desiccation stress. Under these conditions, resident microbes form biofilms which act as optimal surfaces for oyster spat attachment and growth (Campbell et al., 2011; Nold and Ward, 1996). Under lower irradiance and desiccation stress, as on the surface of a fully submerged reef ball, biofilm formation and associated resources for oyster growth are minimal. **Here, we set out to determine whether there is a relationship between the chemical and/or taxonomic composition of biofilms and oyster spat growth under intertidal versus subtidal conditions. We further investigate the N cycling dynamics of biofilms under these two conditions to inform the interplay between biofilm communities, oyster growth, and N remediation.**

Biofilms are communities of microbes enveloped by extracellular polymeric substances (EPS), primarily polysaccharides and proteins (Stolz, 2000). They are globally ubiquitous, but more prevalent in intertidal environments (Stal and Caumette, 2013). It is generally accepted that the presence of mats supports oyster larvae attachment and growth, via either microbial chemical cues or the physical properties of EPS (Rato et al., 2025). Previous research on *Crassostrea vir-*

ginica larvae in the Chesapeake Bay suggests a positive relationship between the age and mass of biofilm on surfaces and successful spat settlement (Campbell et al., 2011). While (Campbell et al., 2011) report a positive relationship between specific taxa of microbes and successful settlement and growth, the methods used could not determine their specific taxonomic identities. It is debated whether biofilms enhance spat success due to specific chemicals excreted by specific microbes, or whether the general compounds present in all fully developed mats, regardless of taxonomic composition, have physical properties that promote attachment (Rato et al., 2025).

Biofilm EPS contain different compounds under varying environmental conditions. Under high irradiance, biofilm are typically composed of photosynthetic microbes (e.g. cyanobacteria and diatoms) excreting primarily polysaccharides, while under low irradiance, mats contain a mix of photosynthetic and non-photosynthetic microbes excreting a more diverse set of compounds, including protein (Gonzalez-Nayeck et al., 2022, 2023). EPS containing a higher proportion of polysaccharide has a greater adhesive strength (Harimawan and Ting, 2016). **As such, we hypothesized that the surfaces of intertidal miniature reef balls would contain relatively more photosynthetic microbes excreting "stickier" substances than subtidal miniature reef balls, and that this "stickier" surface would better promote attachment and growth of oyster spat.**

Oyster shell biofilm typically contains bacteria that convert ammonium (NH_4^+) to nitrate (NO_3^-), while the microbiome of the oyster gut typically contains denitrifying bacteria (Ray et al., 2019). Furthermore, many cyanobacteria fix atmospheric N (Stal, 2015). As such, understanding the interplay between these two communities and the overall balance of N-N cycling processes is important towards understanding whether oyster-associated biofilm net promotes excess N remediation (by supporting oyster growth) or limits excess N remediation (by acting as a source of N).

Here, we test our hypotheses by incubating cured oyster shells alongside the miniature reef balls in the Park's Gansevoort Peninsula over the course of the 2025 growing season. At the end of the growing season, we sampled to determine the taxonomic compositions of microbial communities on both the reef balls and the shells. We then harvested the shells to measure N

fluxes during incubation and determine the bulk, carbohydrate, and protein content of biofilm EPS. Results suggest that photosynthetic microbes are relatively more abundant in intertidal biofilm communities, but that differences in oyster growth between intertidal and subtidal reef balls may be more related to hypoxic conditions experienced by the reef balls rather than EPS content.

Methods

Experimental setup and sampling strategy

A goal of our sampling strategy was to test non-destructive methods for sampling oyster ecological conditions. Cured oyster shells, intended to mimic the natural surfaces on reef balls, were provided by Park research staff. Three cured shells each (n=12 total) were attached to four miniature reef balls in the eastern (reef balls 2 and 3, intertidal condition) and western (reef balls 4 and 5, subtidal condition) inflow channels to the reconstructed Gansevoort Salt Marsh on June 5th, 2025. The shells were attached using zip ties to thick cable wires on the reef balls, and an additional zip tie was placed underneath the shell to keep it in place (Figure 1). Differences in irradiance between intertidal and subtidal conditions were confirmed via an MQ-510: Full-Spectrum Quantum Meter with Underwater Sensor (Apogee Instruments, Logan, UT, USA). The shells and reef balls were left to incubate in the river for 139 days, removed once monthly for oyster growth monitoring, and harvested on October 22nd, 2025. Unfortunately, the additional zip ties were insufficient to keep the shells in place, which migrated to the base of the reef balls mid-experiment; as such, we consider the shells to reflect only the conditions at the base of each reef ball. The three live oysters included in the N flux incubation measurements described below were sampled only from reef ball 4 as to minimize oyster casualty. One additional oyster was accidentally dislodged from reef ball 5 during harvesting and was included in the incubations as well.

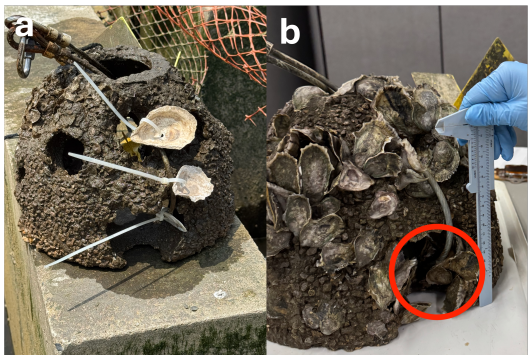

Figure 1 Cured oyster shells attached to a subtidal reef ball prior to incubation (**a**). Photograph by author June 5th, 2025. Location of cured oyster shells after incubation indicated by red circle (**b**). Photograph by author October 22nd, 2025.

N flux incubations

Seawater (salinity = 24 ppt) from the Hudson River was collected in multiple 20 L carboys from the dock at Pier 40 on the same day as shell collection. Shells and live oyster samples were placed in polycarbonate tubes (30 cm x 7.6 cm), kept in a dark cooler, and immediately transported with the seawater to the laboratory. All tubes were slowly filled with 230 ml of seawater and then fitted with a gas tight lid with an inflow and outflow line. Continuous-flow sediment core incubations (Gardner and McCarthy 2009) were performed by pumping site water through the cores with a peristaltic pump at a rate of 1.25 ml min^{-1}. The cores were held in a dark environmental chamber at 17°C during the incubation, which was the same temperature as the river at time of collection. After 18 h of continuous-flow through the cores, sample collection was performed. Inflow and outflow samples for nutrient analysis were collected in triplicate by filtering the seawater through a 0.2 μm nylon syringe filter (Thermo Scientific, Rockwood, Tennessee, USA) into 20 ml scintillation vials. Vials were stored at -20°C until analyzed. Triplicate outflow samples for gas analysis were collected in 12 ml exetainer sample vials (Labco Ltd., Lampeter, United Kingdom) by placing the outflow line direct into the vial and letting it overflow for several volumes. Inflow samples were transferred with the syringe and tubing into the bottom of the exetainer vials with overflow. All gas samples were given 200 μl of zinc chloride, capped with no air bubbles, and stored underwater at 4°C until analyzed.

Shell and live oyster incubation samples (i.e., inflows and outflows) were analyzed for nitrate (NO_3^-) + nitrite (NO_2^-) (collectively known as NO_x^-) fluxes. Measurements were performed on a SealAQ300 discrete analyzer (Seal Analytical Inc., Mequon, Wisconsin, USA). NO_x^- was measured using the sulfanilamide method with cadmium reduction while NO_2^- was measured with the sulfanilamide method without cadmium reduction (APHA 1998). Shell and live oyster incubation samples collected for gas analysis were measured with membrane inlet mass spectrometry (MIMS; Bay Instruments, Easton, MD, USA; Kana et al. 1994) which quantifies the concentrations of $^{28}N_2$, $^{32}O_2$, and ^{40}Ar that can be used to calculate net N_2 fluxes and sediment oxygen demand. A standard, made with artificial seawater of the same salinity as the samples, was held in a water bath

at 17°C and equilibrated to atmospheric gases by low-speed stirring. The standard was measured alongside all samples to correct for instrument drift. To calculate the gas and nutrient fluxes (μmol element m^{-2} h^{-1}), the outflow concentrations were subtracted from the inflow concentrations and this value was then multiplied by the flow rate (1.25 ml min^{-1}) and divided by the core surface area (0.003957 m^{-2}). Net shell/live oyster uptake of the nutrient or gas was indicated by negative fluxes while a release of the nutrient or gas into the water column was indicated by a positive flux. The calculated N_2 fluxes are considered a net flux since denitrification and N fixation were likely co-occurring (Fulweiler et al. 2013). A positive net N_2 flux would indicate that denitrification was the dominant process while a negative net N_2 flux would indicate that N fixation was the dominant process.

EPS Composition

Post-incubation shells with adhered substrate were frozen at -80°C immediately after the incubation period and prior to EPS extraction. Frozen shells were lyophylized prior to analysis using a FreeZone Lyophylizer (Labconco, Kansas City, MO, USA) and shell size was quantified using standard morphometric measurements (Marcus, 1990). EPS was extracted from whole shells using prior methods (Gonzalez-Nayeck et al., 2023; Moore et al., 2021) modified for the large shells. Briefly, whole shells were placed in acid-washed Nalgene bottles and filled with a solution of 0.25 M NaCl until the entire shell surface was covered. Bottles were vortexed for 10 minutes, incubated at 60°C overnight, vortexed again, and the supernatant containing EPS was collected into pre-weighed conical tubes. Ice-cold (4°C) 100% ethanol was added in a 1:1 ratio and placed at 4°C overnight to precipitate EPS. Precipitated EPS was centrifuged and the ethanol removed by evaporation under N_2 gas, and all conical tubes from the same shell sample were combined into one via serial centrifugation. The tube containing combined EPS was weighed once EPS was dry to determine bulk EPS dry weight content. Total carbohydrate protein contents were quantified from triplicate subsamples of dried EPS of variable weights (0.2-0.6 mg) using a phenol and sulfuric acid assay (Zavřel et al., 2018) and Bradford assay (Kielkopf et al., 2020), respectively. Bulk EPS was normalized to cross-sectional shell area approximated as an ellipse using shell length and

width.

Microbial community composition

Immediately prior to harvesting shell samples on October 25th, 2025, samples for 16S (bacterial) and 18S (eukaryotic) rRNA amplicon sequencing were taken via sterile swab by rotating the swab on the intended substrate for 30 seconds. Swabs were immediately placed in sterile 2mL cryogenic vials on ice and transported to the laboratory within 2 hours of collection, where they were kept at $-80°$C prior to DNA extraction. Samples were taken from reef ball surfaces without oysters (henceforth "surface"), from the surfaces of live oyster shells (henceforth "oyster"), and from the surfaces of experimental shells (henceforth "shells"). Each sample type was taken in triplicate from random locations above and below the horizon indicated by Figure 2, for a total of three "top" samples and three "bottom" samples per substrate type, with the exception of reef ball 2 which had 0 oysters on the bottom half of the reef ball. Shells were swabbed both pre-incubation and post-incubation to test the effect of flow-through incubation on microbial composition metrics and to test the validity of using post-incubation samples for EPS carbohydrate content measurement.

DNA was extracted using a DNeasy PowerSoil Pro Kit (Qiagen, Germantown, MD, USA) by following manufacturer instructions and extracted DNA was sent to the Integrated Microbiome Resource Center at Dalhousie University for full-length 16S and 18S amplicon sequencing on a PacBio Vega (Pacific Biosciences, Menlo Park, CA, USA) and for initial library preparation, denoising and taxonomy assignments using standardized protocols and workflows (Comeau et al., 2017). Results for successful samples ($>$500 reads, n= 65/69 samples submitted) were provided in the form of Amplicon Sequence Variants (ASVs) with assigned taxonomy for each sample. A summary of successful samples is provided in Table Appendix B.1.

Post-processing and statistical analyses were implemented in R (R Core Team, 2025) using the workflow described in the Microbiome Helper (Comeau et al., 2017) wiki page titled "Microbiome Helper 2 Analysis workflow in R," and debugged/edited using the large language model Claude (Anthropic, 2024). R packages used included phyloseq (McMurdie and Holmes, 2013) to manipulate microbiome data structures and conduct alpha diversity analyses, vegan (Oksanen et

al., 2025) to create the rarefaction curves and conduct beta diversity analyses, AlDEx2 (Fernandes et al., 2014) as the primary differential abundance [DA] analys tool, MaAsLin3 (Mallick et al., 2021) to validate DA analyses, and ggplot2 (Wickham, 2011) to make figures.

ASVs with fewer than 10 reads and/or present in fewer than 5% of total samples were filtered out to avoid sparsity-related issues when working with compositional data (Nikodemova et al., 2023). Post-incubation shells were filtered out of all analyses except for the specific pre/post incubation analysis to avoid false replication errors. A rarefaction curve was generated (Figure Appendix A.2) to identify and filter samples with shallow read depths. While a visual analysis suggests a conservative depth cutoff would be from 2,000-5,000 reads, this would eliminate an entire technical subset (for 16S: reef ball 2 surface, 1184, 1541 and 1591 reads), and 1000 reads has been cited as a reasonable threshold (Comeau et al., 2017; Weiss et al., 2017). We do not rarefy the data in order to maintain all features and because both the vegan package and the ALDEx2 package consider the depth of the data explicitly when calculating beta diversity and DAs (McMurdie and Holmes, 2014). Differentially abundant genera were considered robust when identified by both ALDEx2 and Maaslin3 (Comeau et al., 2017) with the exception of shells pre and post incubation where only ALDEx2 results are used because MaAasLin3 cannot support paired data with only two samples per pair. Relative abundances (reads per ASV/all reads) were labeled as rare ($< 0.1\%$), moderate ($0.1 - 1\%$), and abundant ($> 1\%$).

Results

Characteristics of reef balls and oyster growth

Photon flux density (irradiance) was measured at the start of the incubation (June 5th, 2025 around 2:50 pm) confirming that intertidal reef balls received approximately 70 μmol photons m^{-2} s^{-1} throughout the height of the reef ball (while exposed) while subtidal reef balls received 18 and 0 μmol photons m^{-2} s^{-1} of light immediately below the water surface and 0.27 m below the surface, respectively.

The oysters on reef balls 2, 3, 4, and 5 grew significantly ($p<0.001$) throughout the season, with increases in average length (mm) of 177.2%, 163.5%, 156.3% and 160.5%, respectively (Hudson River Park Trust, River Project, 2025). Average increases in oyster length were statistically insignificant between individual reef balls (ANOVA $p = 0.2739$) and when averaged into subtidal and intertidal sets (Welch's t-test $p = 0.0782$). While the number of oysters counted on each reef ball was relatively consistent at harvest time (n = 58, 58, 58 and 60), oysters on the subtidal reef balls were sparse (reef ball 2) or completely absent (reef ball 3) near the base (Figure 2).

Figure 2 Clockwise: Reef ball 2 (**a**; subtidal treatment), Reef ball 3 (**b**; subtidal treatment), Reef ball 4 (**c**; intertidal treatment), Reef ball 5 (**d**; intertidal treatment). Red line indicates the horizon approximately 120 mm from the bottom of each submerged reef ball below which oysters are absent or extremely sparse. Photograph by author October 22, 2025.

N flux measurements

N_2 gas flux measurements from the shell and live oyster incubations show net N fixation by subtidal shells, intertidal shells, and live oysters, with no differences in rates across treatments (Figure 3). NO_3^- fluxes from the same incubations showed differences between subtidal shells and live oysters, with average values indicating net release of NO_3^- in the subtidal shells, net zero NO_3^- flux in the intertidal shells, and net removal of NO_3^- in the live oysters (Figure 3).

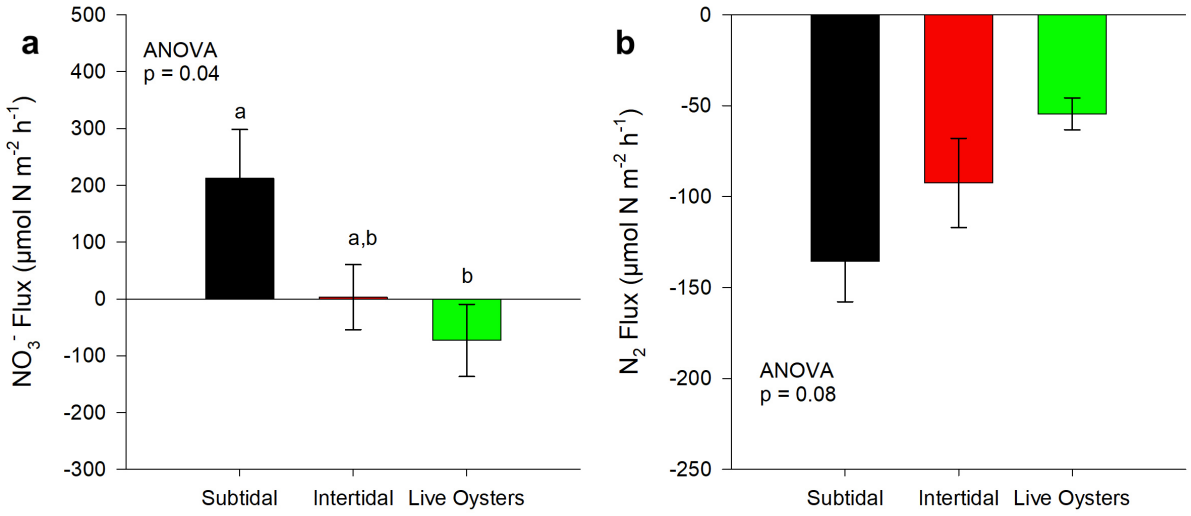

Figure 3 NO_3^- (**a**) and N_2 gas (**b**) flux measurements from shell and live oyster incubations. Treatments sharing a letter are not significantly different based on pairwise Wilcoxon post-hoc tests.

Due to instrument constraints, we were unable to measure NH_4^+ fluxes in the incubations. As such, we are unable to relate these values to specific N cycling processes. However, a mass balance of the average values in each treatment (N fixation minus any nitrate removed) suggests that the shell microbiomes add new nitrate to the water column while the live oysters assimilate (remove) nitrate from the water column in excess of any nitrate added via fixation.

Relative microbial community composition between sample types

Metadata for each sample is shown in Table Appendix B.6. Stacked bar charts showing relative abundances of the top 20 ASVs grouped by phylum per each sample can be found in Figure Appendix A.3 for the bacterial community (16S amplicon sequencing) and in Figure Appendix A.4 for the eukaryotic community (18S amplicon sequencing). Given that the eukaryotic data is contaminated with DNA from transient non-biofilm associated phyla (e.g., *Nematozoa*), we only compare diversity measures for the bacterial community, and we treat eukaryotic results as indicators of relative presence or absence of microbial taxa under different conditions rather than a robust measure of relative abundance.

While median bacterial alpha diversity measures (Richness, Shannon and Simpson) were

not statistically different (p = 0.85, 1.00 and 0.26, respectively) between oyster, shell or surface samples (Figure Appendix A.5a), the sample types were significantly different (p = 0.001) in beta diversity (Bray-Curtis distance; Figure Appendix A.5b). This suggests that each sample type had similar levels of diversity but represented distinct microbial communities. DA analysis detected 4 ASVs robustly enriched in oyster relative to surface samples, including 2 moderately abundant and 2 rare ASV (Table Appendix B.2, Table Appendix B.3). Surface samples had 1 relatively abundant cyanobacterial ASV (*Pleurocapsa PCC 7319*, 2.57% of total reads) relative to shell samples (Table Appendix B.2). There were no differentially abundant ASVs in oysters relative to shell samples (Table Appendix B.2).

Relative bacterial community composition between pre and post incubation samples

Alpha diversity as measured by richness was weakly significantly higher (p = 0.03) for shells post incubation, but not different when considering evenness and dominance (Shannon p = 0.41, Simpson p = 0.46, Figure Appendix A.6a), suggesting that the increase in richness is driven by few rare taxa. Similarly, shells are only weakly different (p=0.016) in Bray-Curtis distance post incubation (Figure Appendix A.6b). One moderately abundant (Genus *Poseidonibacter* 0.24%) ASV was identified by ALDEx2 as being enriched in post-incubation shells.

Relative bacterial community composition between subtidal surface top and bottom

Given that oyster growth appeared limited in the bottom half of subtidal reef balls (Figure 2), we also compared microbial community composition on the surface of the top versus bottom half of subtidal reef balls. Oyster substrate samples were not included in this analysis because only reef ball 2 had oysters in that location. As such, these results should be treated cautiously due to low sample size (n = 6 samples per group). All alpha diversity measures gave statistically insignificant differences between top and bottom surface samples (Figure Appendix A.8a), but beta diversity (Bray-Curtis distance) was moderately (p = 0.01) different (Figure Appendix A.8b), suggesting different community composition. However, neither ALDEx2 nor MaAsLin3 identified differentially abundant ASVs between top and bottom samples.

Relative bacterial community composition between intertidal and subtidal reef balls

Subtidal reef balls had moderately significant higher richness ($p = 0.002$) and highly significant higher Shannon diversity ($p < 0.001$), but were indistinguishable in Simpson diversity ($p = 0.12$) (Figure Appendix A.7a). This suggests that the differences in alpha diversity seen between intertidal and subtidal reef balls is primarily driven by differences in rare taxa. Bray-Curtis distance was significantly ($p = 0.001$) different between intertidal and subtidal reef balls (Figure Appendix A.7b). In support of the alpha diversity results, we identified 98 ASVs robustly enriched in intertidal reef balls (Table Appendix B.4) and 56 ASVs robustly enriched in subtidal reef balls (Table Appendix B.5), but only three of these were relatively abundant (Genera *Pleurocapsa PCC 7319*, 4.06%; an uncultured taxa family *Saprospiraceae*, 1.51%, *Aquimarina*, 1.07%; all enriched in intertidal samples).

Relative eukaryotic community composition between intertidal and subtidal reef balls

While contamination from transient eukaryotic organisms prevented us from directly comparing the biofilm-associated eukaryotic communities on intertidal and subtidal reef balls, we do note that the abundant ($> 1\%$ of reads) genera belonging to the photosynthetic phyla *Diatometa* and *Chlorophyta* are robustly enriched in intertidal samples (Table Appendix B.7).

Preliminary Results for Extracellular Polymeric Substances Composition

As a preliminary test, we extracted bulk dry weight EPS from one subtidal shell (reef ball 3) and one intertidal shell (reef ball 4). The subtidal shell surface contained 0.056 mg mm^{-2} of EPS while the intertidal shell surface contained 0.002 mg mm^{-2} of EPS. Further results, including bulk EPS content for remaining shells, as well as EPS carbohydrate and protein content will be provided in a future addendum to this report.

Discussion

Validity of non-destructive sampling

A goal of this work was to test the validity of using cured oyster shells as proxies for the reef ball surface and/or oyster shell surfaces, in order to have the quantity of material required for

EPS composition analyses without sacrificing live oysters or removing beneficial biofilm from the reef balls themselves. While shells had a distinct microbial composition (Figure Appendix A.5b), this appears to have been driven primarily by one differentially abundant taxon, *Pleurocapsa PCC 7319*, on the surface relative to the shells (Table Appendix B.2). Given that *Pleurocapsa PCC 7319* is a Cyanobacteria, this is potentially due to the fact that the shells migrated to the interior of the reef balls during the experiment (Figure 1) and were light-limited. While it is encouraging that there were no differentially abundant taxa between experimental shells and live oyster shells, future attempts at this method should emphasize keeping the shells in place on the outer surface of the reef ball.

We further questioned whether it was valid to analyze the biofilm on the shells post continuous-flow incubation. While shells pre and post incubation had different community compositions according to beta diversity analyses, this was only weakly significant ($p = 0.02$) and primarily driven by one differentially abundant taxon that was only moderately abundant (Genus *Poseidonibacter* 0.24%; Table Appendix B.2). We do note that members of *Poseidonibacter* are known N-fixers and can convert NO_3^- to NO_2^- (Pérez-Cataluña et al., 2018), so it is plausible that conditions in the continuous-flow incubation selected for N fixation (we emphasize, however, that it only represented 0.24% of shell reads).

N flux measurements

Our result that live oysters removed NO_3^- in excess of NO_3^- added via fixation while shell communities added NO_3^- to the water column aligns with prior literature (Ray et al., 2019 and references within), with the caveat that Ray et al., 2019 specifically attribute added N to nitrification rather than N fixation. Our N_2 fluxes confirm that shell and oyster communities displayed net N fixation, but given our lack of NH_4^+ data, we can't confirm whether shell communities adding NO_3^- to the water column are removing excess NH_4^+ in the process. Given that phytoplankton in the HRE are co-limited by light and NH_4^+ (Dianne I. Greenfield, 2023), future work should clarify this distinction.

While it was not statistically significant, subtidal shells on average contributed more NO_3^-

to the water column than intertidal shells (Figure 3). Qualitatively, subtidal samples appear to have relatively more samples containing ASVs mapping to the phylum Nitrospirota (Figure Appendix A.3), which are known NO_2^- oxidizers (Daims et al., 2001).

Intertidal vs. subtidal

Our original hypothesis was developed to explain the near total mortality seen in intertidal relative to subtidal reef balls in 2024 (Hudson River Park Trust, River Project, 2024). We hypothesized that biofilm on intertidal surfaces would harbor relatively more photosynthetic microbiota, producing relatively more biofilm by mass which in turn supports spat attachment and growth. Two results in 2025 cause us to reject our original hypothesis: near identical growth on intertidal and subtidal reef balls (Hudson River Park Trust, River Project, 2025), and preliminarily, relatively higher EPS concentrations on subtidal surfaces. EPS-producing Cyanobacteria, diatoms (*Diatometa*) and green algae (*Chlorophyta*) were robustly enriched on intertidal surfaces (Tables Appendix B.4, Appendix B.7). Furthermore, frequent shear forces promote EPS production as a protectant strategy for biofilm microbiota (Naik et al., 2023; Yu et al., 2025), and the diatom genus *Melosira*, cited as a particularly shear-tolerant genus, was robustly more abundant on intertidal surfaces (Naik et al., 2023). However, this doesn't correspond to a greater dry weight mass of EPS per mm^2.

In revising our hypothesis, we hoped to address the apparent depth preference observed on the subtidal reef balls, where the majority of oyster growth was observed above the maximum depth of light penetration. While we did not find any robust DA genera between the top and bottom of subtidal reef ball surfaces, we note that the second most abundant robustly enriched ASV on subtidal surfaces belongs to the family *Desulfocapsaceae*, comprised only of strict anaerobic bacteria (Table Appendix B.5, Galushko and Kuever, 2015). The relative abundance of these ASVs indicates that the bottom of the subtidal reef balls experience at least transient hypoxia, which could explain the relative absence of oyster growth on these surfaces (Jeppesen et al., 2018). Under suboxic conditions, we would also expect slower rates of heterotrophic degradation of organic matter (Kristensen and Holmer, 2001). As such, we hypothesize that while intertidal surfaces might promote greater EPS *production*, subtidal surfaces promote greater EPS *accumulation* over

time due to rate-limiting suboxic conditions. While the Hudson River does not typically experience hypoxic conditions when measured in the open water column (Dianne I. Greenfield, 2023; Howarth et al., 2006) suboxic microzones can be created in any water column when flow is restricted (Huang et al., 2019), suggesting that the walls and rocks surrounding the subtidal reef balls might be creating areas of restricted flow.

Future work and recommendations for Park planning

The motivation behind this work was to better inform reef ball placement for optimal oyster growth. Given that intertidal and subtidal reef balls saw near identical growth in 2025, preliminarily both intertidal and subtidal placements appear appropriate to promote growth. However, the discovery of at least transient hypoxic conditions at the base of the subtidal reef balls suggests that the Park should ensure that reef ball placement does not limit water flow. Future research at the Park should aim to determine the conditions under which hypoxic microzones are created to further optimize oyster growth on artificial structures.

Acknowledgements

We thank CUNY's Office of Research and the Hudson River Park Trust for supporting this work. We also thank Park researchers and staff Siddhartha Hayes, Michaela Mincone, Carrie Roble, Ivette Evangelista and Toland Kister for their helpful discussions and assistance in arranging for and conducting the field work for this project. Thank you to Allison Fitzgerald for advice on experimental design and to Ilahna Cohen and Theodore Muth for advice on analyzing the amplicon data.

Appendix A Additional Figures

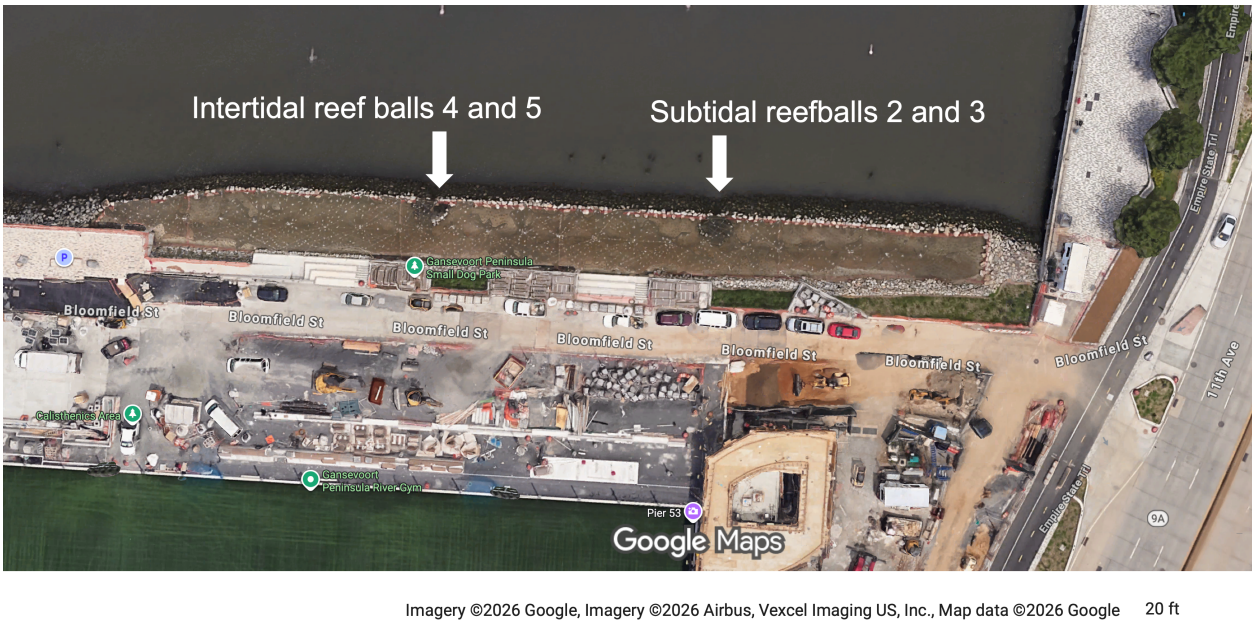

Figure Appendix A.1 Location of intertidal and subtidal mini reef balls within the reconstructed Gansevoort Salt Marsh. Image downloaded from Google Maps in 2026, but image is from earlier (likely 2022) given the state of construction.

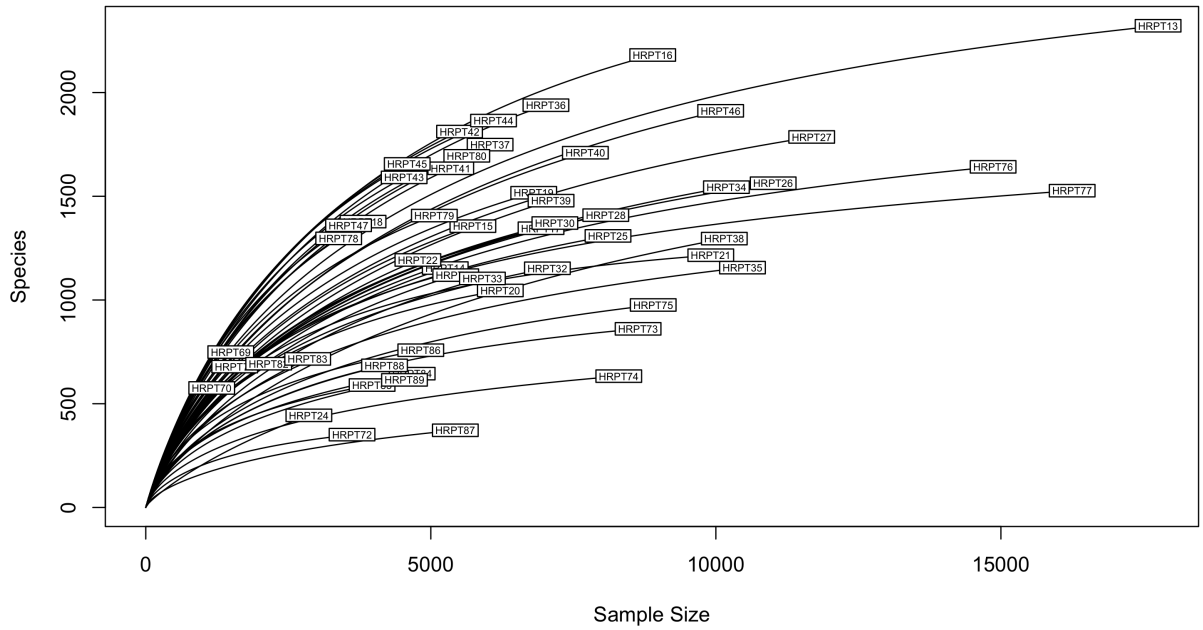

Figure Appendix A.2 Rarefaction curve for samples included in this analysis.

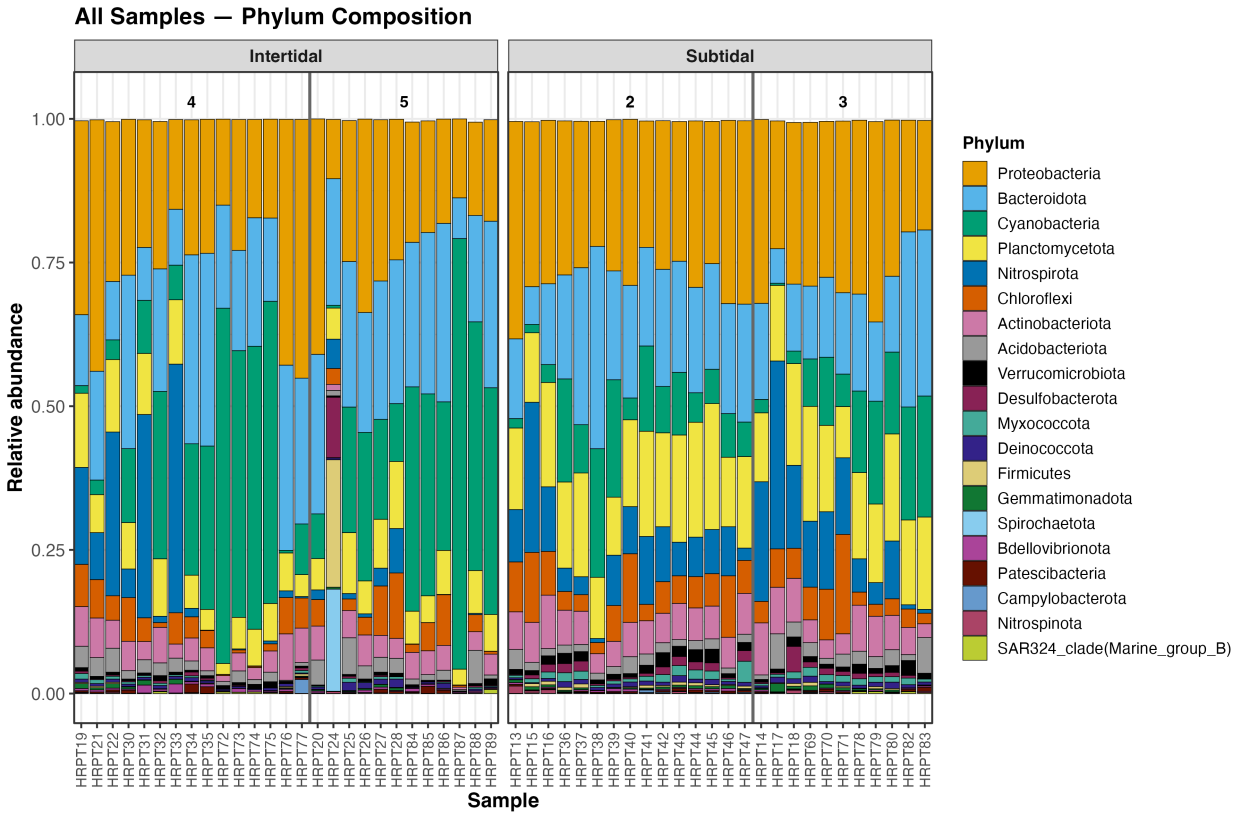

Figure Appendix A.3 Stacked bar chart showing the top 20 ASVs by bacterial phyla across all samples included in this study. Bars that don't sum to 1.00 indicate contributions from ASVs that are not in the top 20.

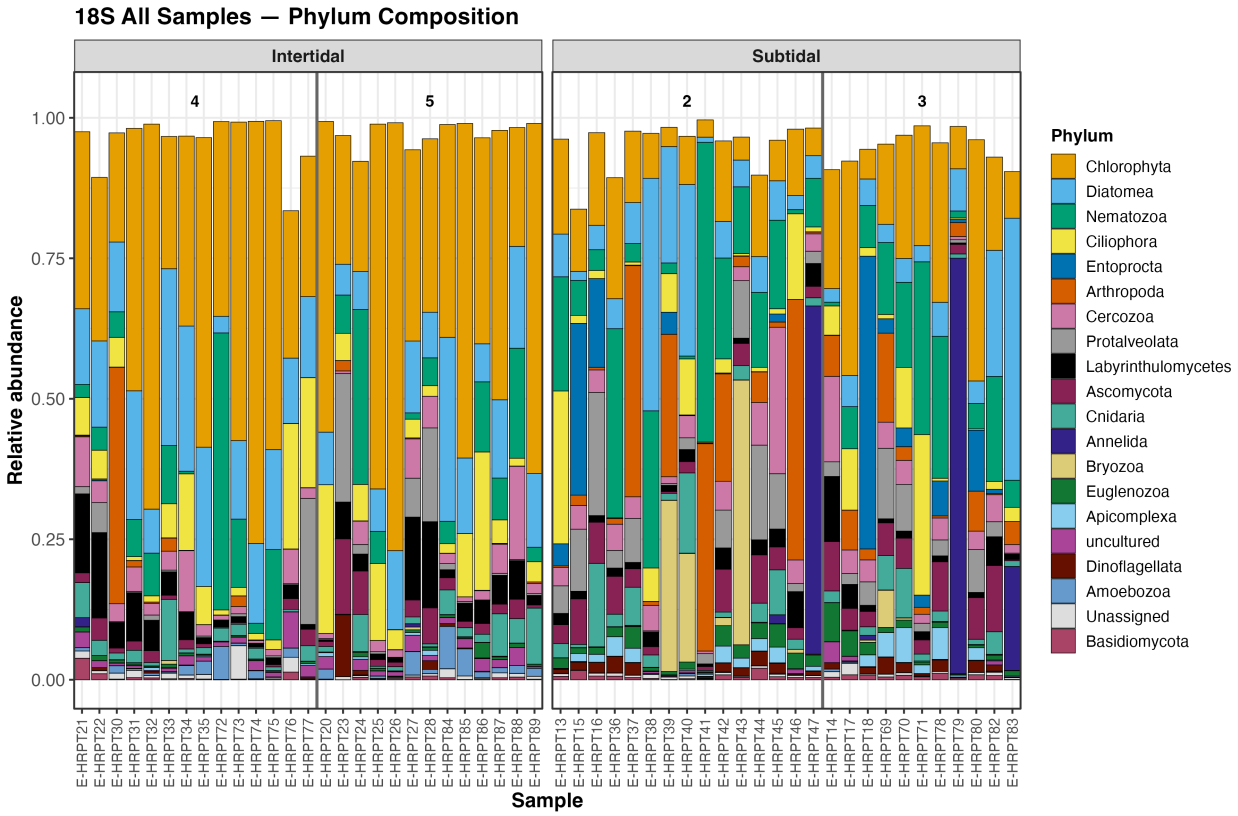

Figure Appendix A.4 Stacked bar chart showing the top 20 ASVs by eukaryotic phyla across all samples included in this study. Bars that don't sum to 1.00 indicate contributions from ASVs that are not in the top 20.

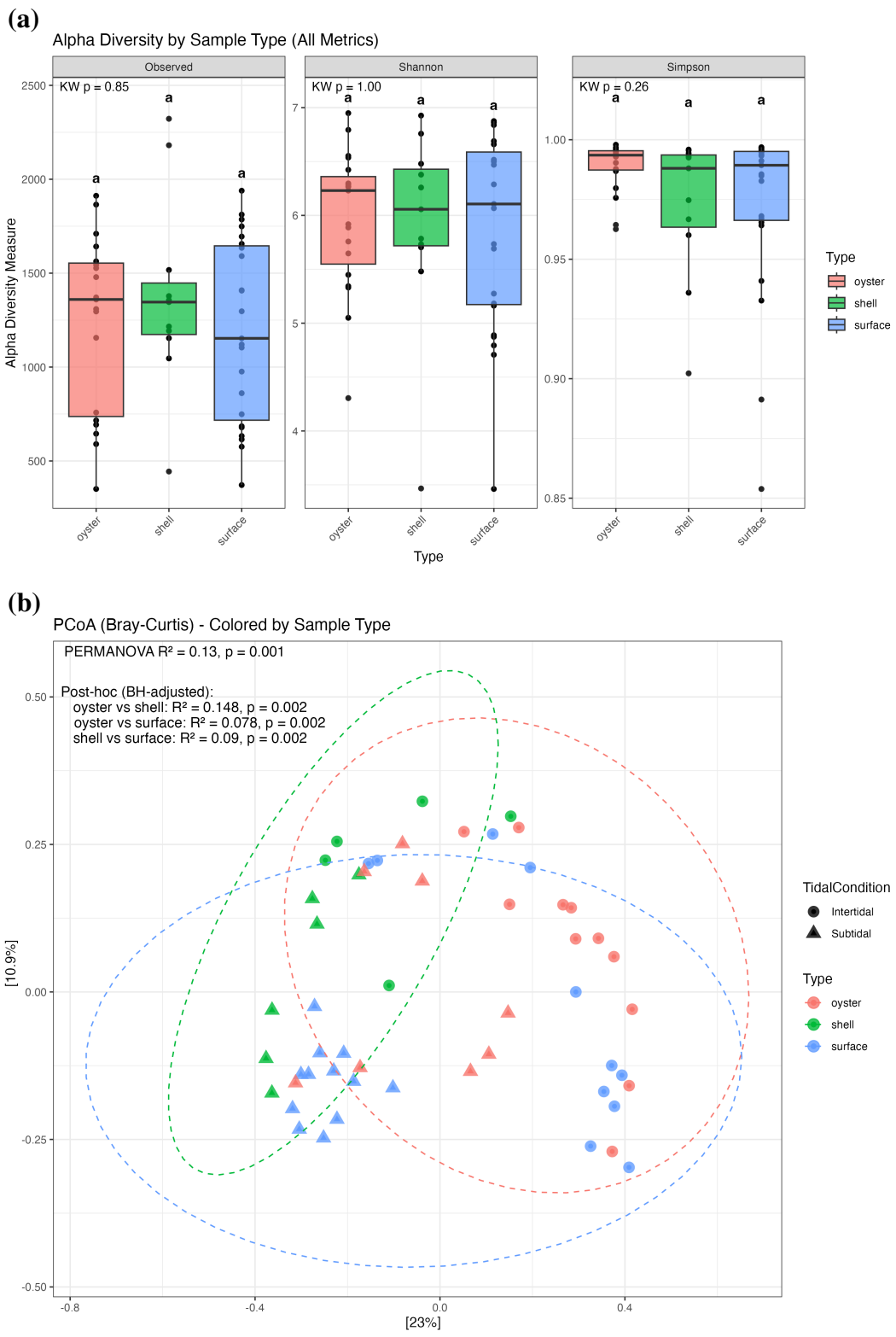

Figure Appendix A.5 Comparison of alpha diversity metrics and community composition by substrate type. (a) Alpha diversity metrics. Treatments sharing a letter are not significantly different based on Kruskal–Wallis tests. (b) Principal Coordinate Analysis (PCoA) in Bray–Curtis space. Colors represent sample type and shapes indicate tidal condition. Statistically significant differences between groups were determined using pairwise PERMANOVA with Holm correction.

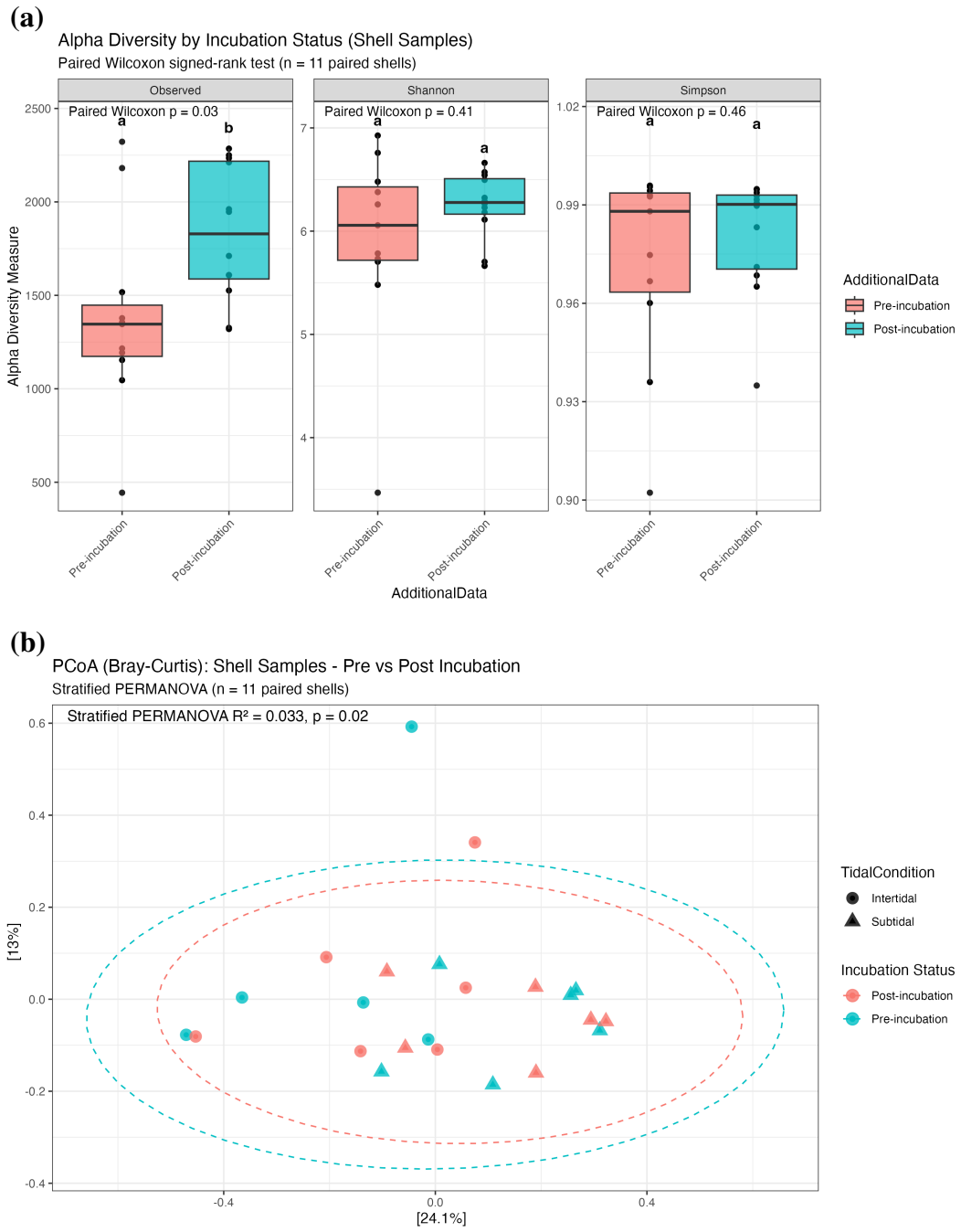

Figure Appendix A.6 Alpha diversity and community composition of shell samples pre- and post-incubation. (a) Alpha diversity metrics. Treatments sharing a letter are not significantly different based on pairwise Wilcoxon post-hoc tests. (b) Principal Coordinate Analysis (PCoA) in Bray–Curtis space. A stratified PERMANOVA was used to account for paired samples.

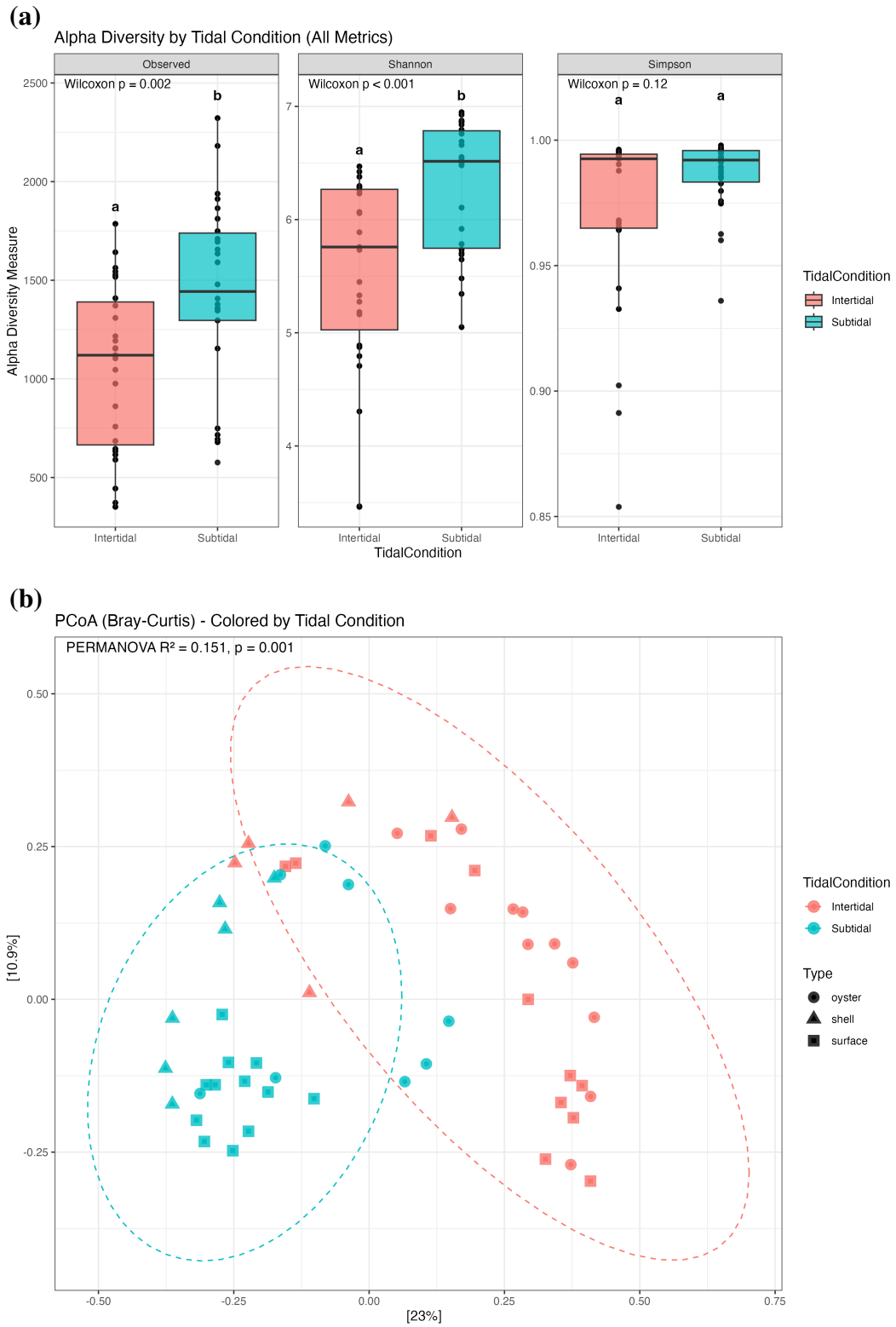

Figure Appendix A.7 Intertidal versus subtidal comparisons. (a) Alpha diversity metrics for pre-incubation shell samples in the intertidal and subtidal treatments. Treatments sharing a letter are not significantly different based on pairwise Wilcoxon post-hoc tests. (b) Principal Coordinate Analysis (PCoA) in Bray–Curtis space. Colors represent tidal condition and shapes indicate sample type.

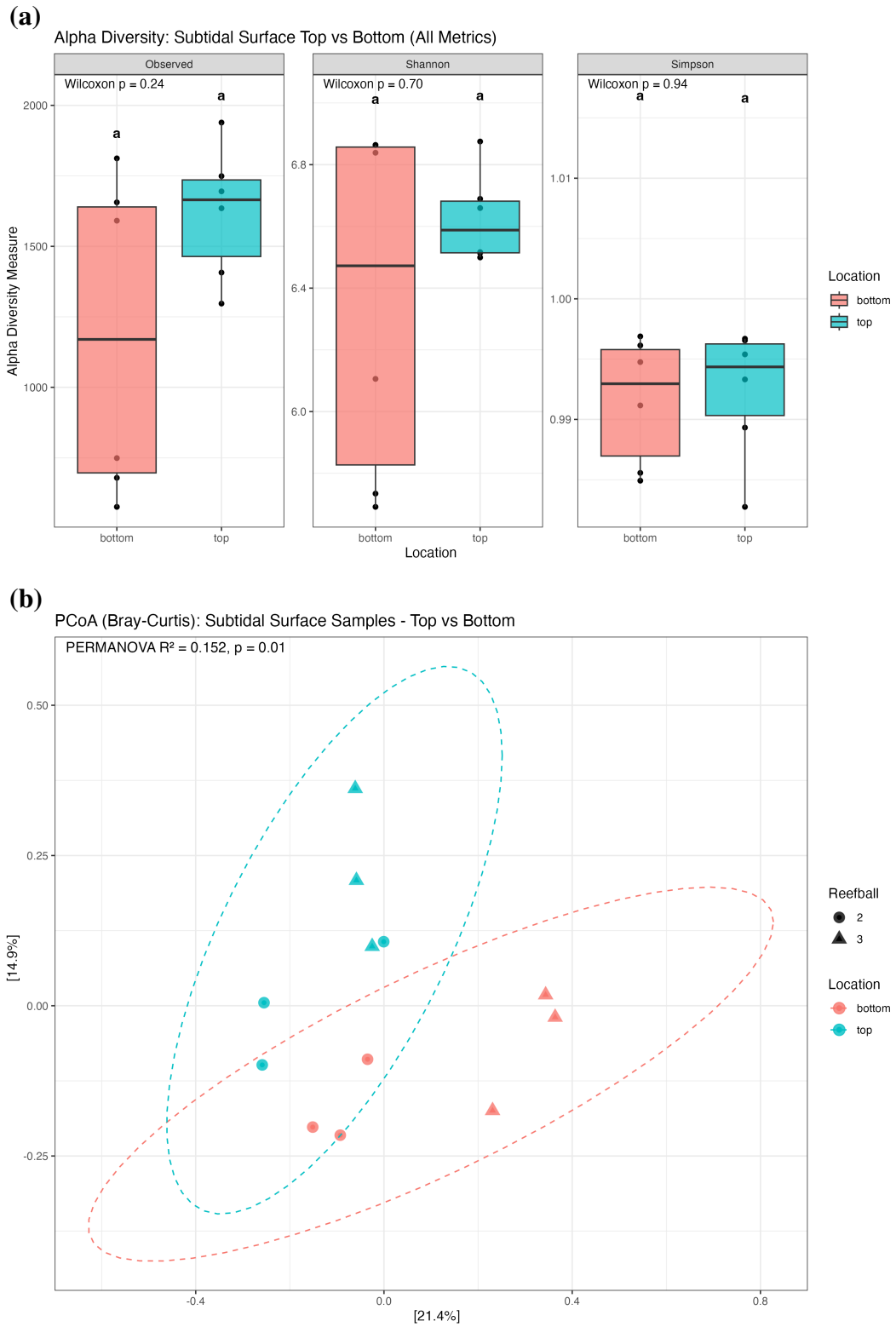

Figure Appendix A.8 Subtidal surface comparisons. (a) Alpha diversity metrics for top versus bottom surface samples in the subtidal treatment. Treatments sharing a letter are not significantly different based on pairwise Wilcoxon post-hoc tests. (b) Principal Coordinate Analysis (PCoA) in Bray–Curtis space comparing top and bottom surface communities.

Appendix B Tables

Table Appendix B.1 Summary of successful 16S rRNA samples by substrate type and tidal condition. Of 69 samples submitted for sequencing, 65 samples passed quality filtering (¿500 reads).

Sample Type	Tidal Condition	n
Shell (Pre-incubation)	Intertidal	6
Shell (Pre-incubation)	Subtidal	5
Shell (Post-incubation)	Intertidal	6
Shell (Post-incubation)	Subtidal	6
Oyster	Intertidal	10
Oyster	Subtidal	9
Surface	Intertidal	12
Surface	Subtidal	11
Total		**65**

Table Appendix B.2 Summary of differential abundance analysis results by comparison. PERMANOVA tests community-level differences (stratified PERMANOVA for Shells Pre vs Post); ALDEx2 and MaAsLin3 identify individual differentially abundant ASVs. Overlap indicates ASVs significant in both methods (robust findings). MaAsLin3 was not run for Shells Pre vs Post (see methods for details).

Comparison	PERMANOVA p-value	ALDEx2	MaAsLin3	Overlap
Intertidal vs Subtidal	0.001	166	499	154
Oyster vs Surface	0.002	10	14	4
Shell vs Surface	0.002	2	4	1
Oyster vs Shell	0.002	5	2	0
Subtidal Surface Top vs Bottom	0.01	0	0	0
Shells Pre vs Post	0.016	1	—	—

Table Appendix B.3 Differentially abundant genera: Oyster vs Surface samples. Genera identified as significant by both ALDEx2 and MaAsLin3 (robust findings). All genera were enriched on oyster substrates relative to reef ball surfaces. Effect size from ALDEx2; negative values indicate oyster enrichment. Sorted by relative abundance.

Genus	Phylum	n ASVs	Rel. Abund. (%)	Effect
Ulvibacter	Bacteroidota	2	0.20	−0.90
Marixanthomonas	Bacteroidota	1	0.13	−0.95
Actibacterium	Proteobacteria	1	0.09	−1.11

Table Appendix B.4 Differentially abundant genera: Intertidal vs Subtidal samples (Part 1 – Intertidal-enriched). Genera identified as significant by both ALDEx2 and MaAsLin3 (robust findings). Negative effect sizes indicate intertidal enrichment. Sorted by relative abundance.

Genus	Phylum	n ASVs	Rel. Abund. (%)	Effect
Pleurocapsa PCC-7319	Cyanobacteria	14	4.06	−0.81
uncultured (Saprospiraceae)	Bacteroidota	9	1.51	−0.03
Aquimarina	Bacteroidota	2	1.07	−0.91
Caldora VP642b	Cyanobacteria	1	0.70	−0.54
Rubidimonas	Bacteroidota	5	0.68	−0.71
Chroococcidiopsis PCC-6712	Cyanobacteria	2	0.54	−0.64
unclassified (Rhodobacteraceae)	Proteobacteria	7	0.50	−0.60
Maribacter	Bacteroidota	4	0.49	−0.87
Schizothrix LEGE 07164	Cyanobacteria	1	0.41	−0.80
Ilumatobacter	Actinobacteriota	6	0.40	−0.31
Actibacterium	Proteobacteria	3	0.38	−0.83
Limibaculum	Proteobacteria	3	0.31	−0.75
Pricia	Bacteroidota	2	0.31	−0.67
Silicimonas	Proteobacteria	3	0.25	−0.62
Jannaschia	Proteobacteria	2	0.23	−0.98
Erythrobacter	Proteobacteria	3	0.20	−0.61
Hoppeia	Bacteroidota	3	0.18	−0.69
Pseudahrensia	Proteobacteria	4	0.17	−0.41
uncultured (Caldilineaceae)	Chloroflexi	2	0.15	−0.79
Filomicrobium	Proteobacteria	1	0.14	−0.78
Ulvibacter	Bacteroidota	2	0.13	−0.79
Psychroserpens	Bacteroidota	3	0.13	−0.84
Yoonia-Loktanella	Proteobacteria	2	0.13	−0.11
Lewinella	Bacteroidota	3	0.11	−0.64
uncultured (Ardenticatenales)	Chloroflexi	1	0.09	−0.71
Fulvivirga	Bacteroidota	1	0.09	−0.62
Phormidesmis ANT.LACV5.1	Cyanobacteria	2	0.08	−0.74
Marixanthomonas	Bacteroidota	1	0.07	−1.01
Rubrivirga	Bacteroidota	3	0.07	−0.62
Truepera	Deinococcota	1	0.06	−0.86
uncultured (Sphingomonadaceae)	Proteobacteria	1	0.06	−0.66
uncultured (Planctomycetales)	Planctomycetota	1	0.06	−0.63
Sva0996 marine group	Actinobacteriota	1	0.05	−0.79
Sulfitobacter	Proteobacteria	1	0.04	−0.72
Blastocatella	Acidobacteriota	1	0.04	−0.63
Nitriliruptoraceae	Actinobacteriota	1	0.03	−0.79
Granulosicoccus	Proteobacteria	1	0.03	−0.67
Litorimicrobium	Proteobacteria	1	0.03	−0.61
Winogradskyella	Bacteroidota	1	0.02	−0.65

Table Appendix B.5 Differentially abundant genera: Intertidal vs Subtidal samples (Part 2 – Subtidal-enriched). Genera identified as significant by both ALDEx2 and MaAsLin3 (robust findings). Positive effect sizes indicate subtidal enrichment. Sorted by relative abundance.

Genus	Phylum	n ASVs	Rel. Abund. (%)	Effect
unclassified (Gammaproteobacteria)	Proteobacteria	1	0.32	+0.71
uncultured (Desulfocapsaceae)	Desulfobacterota	2	0.26	+0.66
Woeseia	Proteobacteria	3	0.24	+0.70
uncultured (Actinomarinales)	Actinobacteriota	4	0.23	+0.73
uncultured (Sandaracinaceae)	Myxococcota	3	0.22	+0.75
Subgroup 10	Acidobacteriota	2	0.19	+0.05
uncultured (Gammaproteobacteria)	Proteobacteria	2	0.16	+0.66
Halioglobus	Proteobacteria	2	0.13	+0.69
Sabulilitoribacter	Bacteroidota	1	0.11	+0.59
uncultured (Hyphomonadaceae)	Proteobacteria	1	0.10	+1.00
Muriicola	Bacteroidota	1	0.10	+0.67
Lutimonas	Bacteroidota	2	0.10	+0.64
Robiginitalea	Bacteroidota	1	0.08	+0.84
Ruegeria	Proteobacteria	1	0.08	+0.76
HOC36	Proteobacteria	1	0.08	+0.66
Eudoraea	Bacteroidota	2	0.08	+0.65
Planctomicrobium	Planctomycetota	2	0.08	+0.62
B2M28	Proteobacteria	2	0.08	+0.59
Fuerstia	Planctomycetota	1	0.08	+0.58
unclassified (Flavobacteriaceae)	Bacteroidota	2	0.08	+0.04
Actibacter	Bacteroidota	1	0.07	+0.74
unclassified (Chitinophagales)	Bacteroidota	1	0.07	+0.59
unclassified (Hyphomicrobiaceae)	Proteobacteria	1	0.06	+0.57
Rhodobacteraceae	Proteobacteria	1	0.04	+0.80
unclassified (Pseudomonadales)	Proteobacteria	1	0.04	+0.73
IheB2-23	Proteobacteria	1	0.04	+0.69
uncultured (Gimesiaceae)	Planctomycetota	1	0.04	+0.62
Candidatus Tenderia	Proteobacteria	1	0.03	+0.76
Yangia	Proteobacteria	1	0.03	+0.72
uncultured (Microtrichaceae)	Actinobacteriota	1	0.03	+0.63
Pir4 lineage	Planctomycetota	1	0.03	+0.59
Gimesia	Planctomycetota	1	0.03	+0.58
uncultured (Microscillaceae)	Bacteroidota	1	0.02	+0.61

Table Appendix B.6 Metadata for 16S rRNA gene sequencing samples collected from Hudson River Park Trust reef balls. Location refers to the relative shell location for shells and the position on the reef ball for oyster and surface samples.

SampleID	Reef ball	Location	Type	Tidal condition	Additional data	Shell ID
HRPT1	2	upper	shell	Subtidal	Post-incubation	1
HRPT2	3	upper	shell	Subtidal	Post-incubation	2
HRPT3	2	middle	shell	Subtidal	Post-incubation	3
HRPT4	2	lower	shell	Subtidal	Post-incubation	4
HRPT5	3	middle	shell	Subtidal	Post-incubation	5
HRPT6	3	lower	shell	Subtidal	Post-incubation	6
HRPT7	4	upper	shell	Intertidal	Post-incubation	7
HRPT8	5	upper	shell	Intertidal	Post-incubation	8
HRPT9	4	middle	shell	Intertidal	Post-incubation	9
HRPT10	4	lower	shell	Intertidal	Post-incubation	10
HRPT11	5	middle	shell	Intertidal	Post-incubation	11
HRPT12	5	lower	shell	Intertidal	Post-incubation	12
HRPT13	2	upper	shell	Subtidal	Pre-incubation	1
HRPT14	3	upper	shell	Subtidal	Pre-incubation	2
HRPT15	2	middle	shell	Subtidal	Pre-incubation	3
HRPT16	2	lower	shell	Subtidal	Pre-incubation	4
HRPT17	3	middle	shell	Subtidal	Pre-incubation	5
HRPT18	3	lower	shell	Subtidal	Pre-incubation	6
HRPT19	4	upper	shell	Intertidal	Pre-incubation	7
HRPT20	5	upper	shell	Intertidal	Pre-incubation	8
HRPT21	4	middle	shell	Intertidal	Pre-incubation	9
HRPT22	4	lower	shell	Intertidal	Pre-incubation	10
HRPT23	5	middle	shell	Intertidal	Pre-incubation	11
HRPT24	5	lower	shell	Intertidal	Pre-incubation	12
HRPT25	5	bottom	oyster	Intertidal	Lab	NA
HRPT26	5	bottom	oyster	Intertidal	Lab	NA
HRPT27	5	bottom	surface	Intertidal	Lab	NA
HRPT28	5	bottom	surface	Intertidal	Lab	NA
HRPT29	5	bottom-oyster	surface-oyster	Intertidal	Lab	NA
HRPT30	4	bottom	oyster	Intertidal	Lab	NA
HRPT31	4	bottom	surface	Intertidal	Lab	NA
HRPT32	4	bottom	surface	Intertidal	Lab	NA
HRPT33	4	bottom	surface	Intertidal	Lab	NA
HRPT34	4	bottom	oyster	Intertidal	Lab	NA
HRPT35	4	bottom	oyster	Intertidal	Lab	NA
HRPT36	2	top	surface	Subtidal	Lab	NA
HRPT37	2	top	surface	Subtidal	Lab	NA
HRPT38	2	top	oyster	Subtidal	Lab	NA
HRPT39	2	top	oyster	Subtidal	Lab	NA
HRPT40	2	top	oyster	Subtidal	Lab	NA
HRPT41	2	top	surface	Subtidal	Lab	NA
HRPT42	2	bottom	surface	Subtidal	Lab	NA
HRPT43	2	bottom	surface	Subtidal	Lab	NA
HRPT44	2	bottom	oyster	Subtidal	Lab	NA
HRPT45	2	bottom	surface	Subtidal	Lab	NA
HRPT46	2	bottom	oyster	Subtidal	Lab	NA
HRPT47	2	bottom	oyster	Subtidal	Lab	NA
HRPT69	3	bottom	surface	Subtidal	Lab	NA
HRPT70	3	bottom	surface	Subtidal	Lab	NA
HRPT71	3	bottom	surface	Subtidal	Lab	NA
HRPT72	4	top	oyster	Intertidal	Lab	NA
HRPT73	4	top	surface	Intertidal	Lab	NA
HRPT74	4	top	surface	Intertidal	Lab	NA
HRPT75	4	top	surface	Intertidal	Lab	NA
HRPT76	4	bottom	oyster	Intertidal	live_oyster13	NA
HRPT77	4	bottom	oyster	Intertidal	live_oyster15	NA
HRPT78	3	top	surface	Subtidal	Lab	NA
HRPT79	3	top	surface	Subtidal	Lab	NA
HRPT80	3	top	surface	Subtidal	Lab	NA
HRPT81	3	top	oyster	Subtidal	Lab	NA
HRPT82	3	top	oyster	Subtidal	Lab	NA
HRPT83	3	top	oyster	Subtidal	Lab	NA
HRPT84	5	top	oyster	Intertidal	Lab	NA
HRPT85	5	top	oyster	Intertidal	Lab	NA
HRPT86	5	top	oyster	Intertidal	Lab	NA
HRPT87	5	top	surface	Intertidal	Lab	NA
HRPT88	5	top	surface	Intertidal	Lab	NA
HRPT89	5	top	surface	Intertidal	Lab	NA

Table Appendix B.7 Differentially abundant 18S genera: Intertidal vs Subtidal samples (Part 1 – Intertidal-enriched). Genera identified as significant by both ALDEx2 and MaAsLin3 (robust findings). Negative effect sizes indicate intertidal enrichment. Sorted by relative abundance.

Genus	Phylum	n ASVs	Rel. Abund. (%)	Effect
Ulva	Chlorophyta	6	11.43	−0.73
Blidingia	Chlorophyta	1	4.41	−1.36
Pseudendoclonium	Chlorophyta	2	4.24	−0.80
Monhysterida	Nematozoa	1	2.36	−0.67
Melosira	Diatomea	1	1.44	−0.58
Luticola	Diatomea	4	0.99	−0.61
uncultured	uncultured	2	0.40	−0.80
Dilabifilum	Chlorophyta	1	0.32	−0.81
Nitzschia	Diatomea	2	0.25	−0.79
Achnanthes	Diatomea	1	0.23	−0.52
Bacillariophyceae	Diatomea	2	0.17	−0.73
uncultured (Thraustochytriaceae)	Labyrinthulomycetes	2	0.12	−0.78
Parvamoeba	Amoebozoa	1	0.08	−0.75
CV1-B1-93	Centrohelida	1	0.06	−0.87
unclassified (Centrohelida)	Centrohelida	1	0.05	−0.73
Fragilaria	Diatomea	1	0.05	−0.79
unclassified	unclassified	1	0.04	−0.77
Ulvophyceae	Chlorophyta	1	0.02	−0.63

Table Appendix B.8 Differentially abundant 18S genera: Intertidal vs Subtidal samples (Part 2 – Subtidal-enriched). Genera identified as significant by both ALDEx2 and MaAsLin3 (robust findings). Positive effect sizes indicate subtidal enrichment. Sorted by relative abundance.

Genus	Phylum	n ASVs	Rel. Abund. (%)	Effect
Syndiniales_Group_I	Protalveolata	2	3.92	+0.78
Barentsiidae	Entoprocta	1	2.35	+1.00
Ophiosphaerella	Ascomycota	1	0.79	+0.60
Thalassiosira	Diatomea	1	0.63	+0.93
Heterocapsa	Dinoflagellata	2	0.20	+0.75
Navicula	Diatomea	1	0.16	+0.77
Notosolenus	Euglenozoa	1	0.15	+0.85
Selenidium	Apicomplexa	1	0.13	+0.83
Scheffersomyces	Ascomycota	1	0.12	+0.86
uncultured (Thecofilosea)	Cercozoa	1	0.11	+0.85
uncultured (Labyrinthulomycetes)	Labyrinthulomycetes	1	0.08	+0.65
Ebria	Cercozoa	2	0.07	+0.73
Duboscquella	Protalveolata	2	0.06	+0.59
uncultured (Peronosporomycetes)	Peronosporomycetes	1	0.06	+0.73
Chaetoceros	Diatomea	1	0.05	+0.69
Amphidinium	Dinoflagellata	1	0.04	+0.76
unclassified (Labyrinthulomycetes)	Labyrinthulomycetes	1	0.04	+0.70
Incertae Sedis (Pleosporales)	Ascomycota	1	0.02	+0.65

References

Anthropic. (2024). Claude [Large language model, version Claude Opus 4.5].

Campbell, A. H., Meritt, D. W., Franklin, R. B., Boone, E. L., Nicely, C. T., & Brown, B. L. (2011). Effects of age and composition of field-produced biofilms on oyster larval setting. *Biofouling*, *27*(3), 255–265.

Coen, L. D., Brumbaugh, R. D., Bushek, D., Grizzle, R., Luckenbach, M. W., Posey, M. H., Powers, S. P., & Tolley, S. G. (2007). Ecosystem services related to oyster restoration. *Marine Ecology Progress Series*, *341*, 303–307.

Comeau, A. M., Douglas, G. M., & Langille, M. G. (2017). Microbiome helper: A custom and streamlined workflow for microbiome research. *MSystems*, *2*(1), 10–1128.

Daims, H., Nielsen, J. L., Nielsen, P. H., Schleifer, K.-H., & Wagner, M. (2001). In situ characterization of nitrospira-like nitrite-oxidizing bacteria active in wastewater treatment plants. *Applied and environmental microbiology*, *67*(11), 5273–5284.

Dianne I. Greenfield, P. (2023, May). *Elucidating linkages between storm events and microbial assemblage diversity in the lower hudson river through genomic and biogeochemical analysis: Implications for climate and water quality forecasts* (Final Report). Hudson River Park Trust.

Fernandes, A. D., Reid, J. N., Macklaim, J. M., McMurrough, T. A., Edgell, D. R., & Gloor, G. B. (2014). Unifying the analysis of high-throughput sequencing datasets: Characterizing RNA-seq, 16S rRNA gene sequencing and selective growth experiments by compositional data analysis [ALDEx2 method for compositional differential abundance analysis; uses centered log-ratio transformation and Monte Carlo sampling]. *Microbiome*, *2*, 15.

Galushko, A., & Kuever, J. (2015). Desulfovibrionaceae. *Bergey's Manual of Systematics of Archaea and Bacteria*, 1–13.

Gonzalez-Nayeck, A. C., Grim, S. L., Waldbauer, J., Dick, G. J., & Pearson, A. (2023). Isotopic signatures of carbon transfer in a proterozoic analogue microbial mat. *Applied and Environmental Microbiology*, *89*(5), e01870–22.

Gonzalez-Nayeck, A. C., Mohr, W., Tang, T., Sattin, S., Parenteau, M. N., Jahnke, L. L., & Pearson, A. (2022). Absence of canonical trophic levels in a microbial mat. *Geobiology*, *20*(5), 726–740.

Harimawan, A., & Ting, Y.-P. (2016). Investigation of extracellular polymeric substances (eps) properties of p. aeruginosa and b. subtilis and their role in bacterial adhesion. *Colloids and Surfaces B: Biointerfaces*, *146*, 459–467.

Howarth, R. W., Marino, R., Swaney, D. P., & Boyer, E. W. (2006). Wastewater and watershed influences on primary productivity and oxygen dynamics in the lower hudson river estuary. *The Hudson River Estuary*, *136*.

Huang, J., Hu, J., Li, S., Wang, B., Xu, Y., Liang, B., & Liu, D. (2019). Effects of physical forcing on summertime hypoxia and oxygen dynamics in the pearl river estuary. *Water*, *11*(10), 2080.

Hudson River Park Trust, River Project. (2024, January). *Community oyster monitoring report 2024* (Final Report). Hudson River Park Trust.

Hudson River Park Trust, River Project. (2025). *2025 oyster report* (Final Report). Hudson River Park Trust.

Jacques, P. J. (2017). The origins of coastal ecological decline and the great atlantic oyster collapse. *Political Geography*, *60*, 154–164.

Jeppesen, R., Rodriguez, M., Rinde, J., Haskins, J., Hughes, B., Mehner, L., & Wasson, K. (2018). Effects of hypoxia on fish survival and oyster growth in a highly eutrophic estuary. *Estuaries and Coasts*, *41*(1), 89–98.

Kielkopf, C. L., Bauer, W., & Urbatsch, I. L. (2020). Bradford assay for determining protein concentration. *Cold Spring Harbor Protocols*, *2020*(4), pdb–prot102269.

Kristensen, E., & Holmer, M. (2001). Decomposition of plant materials in marine sediment exposed to different electron acceptors (o2, no3-, and so42-), with emphasis on substrate origin, degradation kinetics, and the role of bioturbation. *Geochimica et Cosmochimica Acta*, *65*(3), 419–433.

Mallick, H., Rahnavard, A., McIver, L. J., Ma, S., Zhang, Y., Nguyen, L. H., Tickle, T. L., Weingart, G., Ren, B., Schwager, E. H., Chatterjee, S., Thompson, K. N., Wilkinson, J. E., Subramanian, A., Lu, Y., Waldron, L., Paulson, J. N., Franzosa, E. A., Bravo, H. C., & Huttenhower, C. (2021). Multivariable association discovery in population-scale meta-omics studies [MaAsLin2/3 method for multivariable association in microbiome studies; supports mixed effects models and multiple normalization options]. *PLoS Computational Biology*, *17*(11), e1009442.

Marcus, L. F. (1990). Traditional morphometrics. *Proceedings of the Michigan morphometrics workshop*, *2*, 77–122.

McMurdie, P. J., & Holmes, S. (2013). Phyloseq: An R package for reproducible interactive analysis and graphics of microbiome census data [R package for microbiome analysis; used for alpha diversity (estimate_richness), beta diversity, and visualization]. *PLoS ONE*, *8*(4), e61217.

McMurdie, P. J., & Holmes, S. (2014). Waste not, want not: Why rarefying microbiome data is inadmissible. *PLoS computational biology*, *10*(4), e1003531.

Moore, K. R., Gong, J., Pajusalu, M., Skoog, E. J., Xu, M., Feliz Soto, T., Sojo, V., Matreux, T., Baldes, M. J., Braun, D., et al. (2021). A new model for silicification of cyanobacteria in proterozoic tidal flats. *Geobiology*, *19*(5), 438–449.

Naik, A. T., Kamensky, K. M., Hellum, A. M., & Moisander, P. H. (2023). Disturbance frequency directs microbial community succession in marine biofilms exposed to shear. *Msphere*, *8*(6), e00248–23.

Nikodemova, M., Holzhausen, E. A., Deblois, C. L., Barnet, J. H., Peppard, P. E., Suen, G., & Malecki, K. M. (2023). The effect of low-abundance otu filtering methods on the reliability and variability of microbial composition assessed by 16s rrna amplicon sequencing. *Frontiers in cellular and infection microbiology*, *13*, 1165295.

Nold, S. C., & Ward, D. M. (1996). Photosynthate partitioning and fermentation in hot spring microbial mat communities. *Applied and Environmental Microbiology*, *62*(12), 4598–4607.

Oksanen, J., Simpson, G. L., Blanchet, F. G., Kindt, R., Legendre, P., Minchin, P. R., O'Hara, R., Solymos, P., Stevens, M. H. H., Szoecs, E., Wagner, H., Barbour, M., Bedward, M., Bolker, B., Borcard, D., Carvalho, G., Chirico, M., De Caceres, M., Durand, S., … Weedon, J. (2025). *Vegan: Community ecology package* [R package version 2.8-0].

Pérez-Cataluña, A., Salas-Massó, N., Diéguez, A. L., Balboa, S., Lema, A., Romalde, J. L., & Figueras, M. J. (2018). Revisiting the taxonomy of the genus arcobacter: Getting order from the chaos. *Frontiers in microbiology*, *9*, 2077.

R Core Team. (2025). *R: A language and environment for statistical computing*. R Foundation for Statistical Computing. Vienna, Austria.

Rato, A., Joaquim, S., Matias, D., & Hubbard, P. C. (2025). The roles of chemical cues in the life cycle of bivalves: Spawning, settlement, and metamorphosis. *Reviews in Aquaculture*, *17*(1), e13007.

Ray, N. E., Henning, M. C., & Fulweiler, R. W. (2019). Nitrogen and phosphorus cycling in the digestive system and shell biofilm of the eastern oyster crassostrea virginica. *Marine Ecology Progress Series*, *621*, 95–105.

Stal, L. J. (2015). Nitrogen fixation in cyanobacteria. *els*, 1–9.

Stal, L. J., & Caumette, P. (2013). *Microbial mats: Structure, development and environmental significance* (Vol. 35). Springer Science & Business Media.

Stolz, J. F. (2000). Structure of microbial mats and biofilms. In *Microbial sediments* (pp. 1–8). Springer.

Weiss, S., Xu, Z. Z., Peddada, S., Amir, A., Bittinger, K., Gonzalez, A., Lozupone, C., Zaneveld, J. R., Vázquez-Baeza, Y., Birmingham, A., et al. (2017). Normalization and microbial differential abundance strategies depend upon data characteristics. *Microbiome*, *5*(1), 27.

Wickham, H. (2011). Ggplot2. *Wiley interdisciplinary reviews: computational statistics*, *3*(2), 180–185.

Yu, S., Lu, X., & Lu, H. (2025). Marine microbial biofilms on diverse abiotic surfaces. *Frontiers in Marine Science*, *12*, 1482946.

Zavřel, T., Očenášová, P., Sinetova, M. A., & Červenỳ, J. (2018). Determination of storage (starch/glycogen) and total saccharides content in algae and cyanobacteria by a phenol-sulfuric acid method. *Bio-protocol*, *8*(15), e2966–e2966.